JOURNAL OF CHEMICAL INFORMATION AND MODELING

Article

pubs.acs.org/jcim

A Cooperative Mechanism of Clotrimazoles in P450 Revealed by the Dissociation Picture of Clotrimazole from P450

Mian Wang,[†,‡,∥] Marc Baaden,[§,∥] Jianyi Wang,[†,*] and Zhiqun Liang[‡,*]

[†]School of Chemistry and Chemical Engineering, Guangxi University, Nanning 530004, China

[‡]College of Life Science and Technology, Guangxi University, Nanning 530004, China

[§]Institut de Biologie Physico-Chimique, Laboratoire de Biochimie Théorique, Centre National de la Recherche Scientifique Unité Propre de Recherche 9080, 13, rue Pierre et Marie Curie, F-75005 Paris, France

Supporting Information

ABSTRACT: The dissociation processes of clotrimazole (CLT) in several models are comparatively investigated by molecular dynamics simulations to explore the cooperative mechanism of clotrimazoles in P450. Our results suggest that when P450 only accommodates the active CLT (CLT1), CLT1 continually diffuses away from heme, and the partial BC loop (residues 73−88) and the extended FG loop (residues 173−186) first close and then open. When the enzyme binds to two CLT molecules, CLT1 basically keeps close to heme, and the partial BC loop and the extended FG loop move close to each other. Clearly, the effector CLT (CLT2) plays a cooperative role in the inhibition of CLT1 on P450. CLT2 restrains the dissociation of CLT1 first through direct $\pi-\pi$ stacking interactions and then through the rearranged binding site induced by CLT2. The presence of CLT1 can help to stabilize the protein structure around CLT2 by interacting with M86, Q173, and M174.

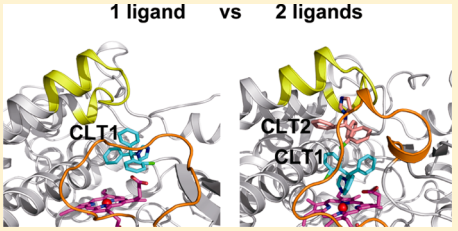

1. INTRODUCTION

Cytochromes P450 (CYPs) are a superfamily of heme-containing enzymes, which can catalyze the biosynthesis of many endogenous compounds, and the oxidative metabolism of numerous endogenous and exogenous compounds.[1,2] P450s are thus recognized as effective targets against related diseases and the major metabolic center of drugs.[2−4] For example, the inhibition of CYP19A1, which can catalyze androgens into estrogens, is helpful to the treatment of estrogen-dependent cancer (such as breast cancer). The inhibition of the fungal form of CYP51A1 can fight against clinical fungal infection. Interestingly, co-administration of ketoconazole (inhibitor of CYP3A4) and Saquinavir (HIV protease inhibitor) is found to reduce the metabolism of Saquinavir and improve the therapeutic effect against HIV infection.[5] The metabolism of Glimepiride is hindered by Amiodarone (inhibitor of P450), causing hypoglycemia.[6] Therefore, it is significant to illuminate the cooperative mechanism of inhibition and the dissociation process of inhibitor from P450 in both medicinal chemistry and pharmacokinetics.

The multiple substrates binding to P450 have been experimentally investigated by many groups.[7−12] For instance, Gilardi and co-workers used the electrochemical method to demonstrate that the simultaneous binding of quinidine and diclofenac can strengthen the inhibition of CYP3A4.[13] Guengerich and co-workers found that the co-occupancy of 1,4-phenylene diisocyanide and 1-isopropoxy-4-nitrobenzene can cooperatively inhibit the catalytic activity of CYP1A2.[14] Miller and co-workers suggested that two 4-methylpyrazoles can simultaneously occupy the binding site of CYP2E1 to inhibit the enzyme activity.[15] Some crystal structures (for example, PDB code 2V0M[16] and 2BDM[17]) provide direct evidence that CYPs can be simultaneously bound by multiple inhibitors. Recently, a species of P450 from *Saccharopolyspora erythraea* (EryK) bound with two clotrimazole (CLT) molecules has been crystallized (PDB code 2XFH).[18] In this structure, the active clotrimazole (CLT1) coordinates to the heme iron with the N3 atom of the imidazole ring, while the effector clotrimazole (CLT2) stacks above the active one (Figure 1A). Note that the two phenyl rings and the chlorophenyl ring of CLT are denoted as Ring A, Ring B, and Ring C, respectively (Figure 1B). Besides, residues 65−95

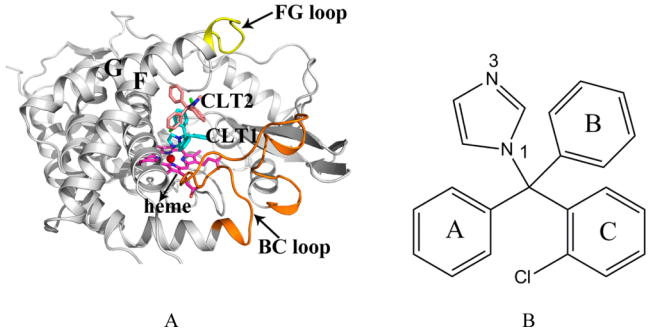

Figure 1. Crystal structure of EryK bound to two CLT molecules (A) and chemical structure of CLT (B).

Received: November 10, 2013
Published: March 11, 2014

 © 2014 American Chemical Society

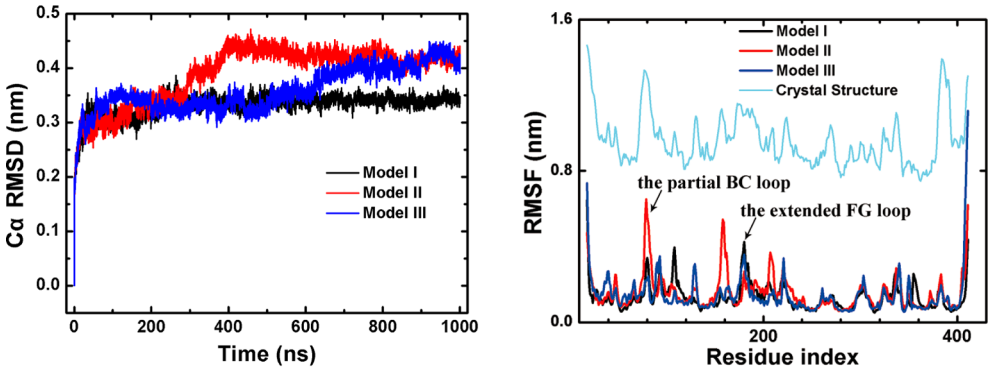

A B

Figure 2. (A) Time dependence of Cα RMSD with respect to their initial structures for model I, model II, and model III, respectively. (B) RMSF of backbone atoms for three systems and crystal structure.

(BC loop), residues 157−175 (F helix), residues 176−182 (FG loop), and residues 183−208 (G helix) are considered as the key regions of governing the open/closed movement of EryK.[19]

Many theoretical efforts were devoted to explore the cooperative mechanisms of multiple substrates in CYPs. For instance, Oostenbrink and co-workers investigated the cooperative binding of two ketoconazole molecules to the CYP3A4 using molecular dynamics (MD) simulation combined with free-energy calculation. They revealed that the binding of the active ketoconazole facilitates the binding of the effector ketoconazole, and the van der Waals interaction is considered as the primary element of binding.[20] The binding of two diazepam molecules to CYP3A4 has been studied by Nussinov and co-workers. They demonstrated that the addition of the effector diazepam helps the active diazepam adopt the favorable orientation to be oxidized through stabilizing F304.[21] Shaik and co-workers have investigated the binding of two diazepam molecules to CYP3A4 using the QM/MM method. They suggested that the two bound diazepams can stabilize compound I (Cpd I), and the effector diazepam can promote the active diazepam approach to Cpd I, thereby favoring oxidation of the active diazepam.[22] Wei and Wang groups have studied the binding of two aniline molecules to CYP2E1. They deemed that the addition of the effector aniline damages the hydrogen bond between T303 and the active aniline, putting the active aniline in an inappropriate position to be oxidized, and it affects the interaction between F478 and the active aniline, positioning the active aniline a little far away from the metabolic center (Cpd I), thus weakening the metabolic efficiency of the active substrate.[23]

However, the dissociation process of CLT from P450 and the cooperative mechanism of CLT molecules are still unclear. To elucidate this, several models are comparatively investigated: the enzyme without any substrate (model I), the enzyme bound to one CLT molecule (model II), and the enzyme bound to two CLT molecules (model III). This work could provide new insights into the inhibition mechanism of multiple substrates and drug−drug interactions in clinical practice and supply a guideline to design novel therapeutic agents against P450 targets.

2. METHODS

The initial structure of model I is generated by deleting two CLT molecules from the crystal structure 2XFH.pdb.[18] Model II is produced by deleting CLT2 from this crystal structure. Model III is derived from this crystal structure.

The molecular dynamics (MD) simulations were carried out with the GROMACS 4.5.5 package[24,25] The GROMOS96 43a1 force field was applied.[26] The interaction parameter file of CLT was constructed by the Automated Topology Builder.[27] For each system, the protein or complex was placed in a rectangular box with a minimal distance of 1.2 nm from the protein to the wall and solvated with SPC water molecules.[28] Counterions were added to maintain an electroneutral system and mimic the physiological environment (75 Na^+ and 48 Cl^- ions for model I, 74 Na^+ and 47 Cl^- ions for model II, and 75 Na^+ and 48 Cl^- ions for model III). Each system was first subjected to steepest descent minimization and then conducted two 100 ps equilibrations. In the first NVT equilibration, the temperature was maintained at 300 K using a velocity-rescaling thermostat[29] with a time coupling constant of 0.1 ps. In the next NPT equilibration, the pressure was maintained at 1 bar by coupling to the Parrinello−Rahman barostat[30] with a time coupling constant of 2.0 ps and isotropic compressibility of 4.5×10^{-5}. Finally, 1 μs molecular dynamics simulation was performed for each system in NPT ensemble with periodic boundary conditions. The LINCS method[31] was used to restrain bond lengths, allowing an integration step length of 2 fs. Electrostatic interactions were calculated using the particle-mesh Ewald algorithm,[32] while a cutoff radius of 1.4 nm was selected for van der Waals interactions.

The relative binding free energy of CLT1 was calculated by the MM-PBSA method.[33,34]

$$\Delta G_{bind} = G_{complex} - G_{receptor} - G_{ligand} \quad (1)$$

$$G = E_{gas} + G_{sol} - T \times S \quad (2)$$

$$E_{gas} = E_{bond} + E_{angle} + E_{torsion} + E_{vdw} + E_{ele} \quad (3)$$

$$G_{sol} = G_{solv,polar} + G_{solv,nonpolar} \quad (4)$$

where E_{gas} is an average energy including bond, angle, torsion, van der Waals, and electrostatic terms from a force field. Solvation free energy G_{sol} is calculated using a numerical solution of the Poisson−Boltzmann equation and an estimation of the nonpolar free energy based on surface area. Both E_{gas} and G_{sol} are obtained by averaging over a sample of similar geometries extracted from a MD trajectory (50 snapshots), and the entropy term was simply neglected.

dx.doi.org/10.1021/ci400660e | J. Chem. Inf. Model. 2014, 54, 1218−1225

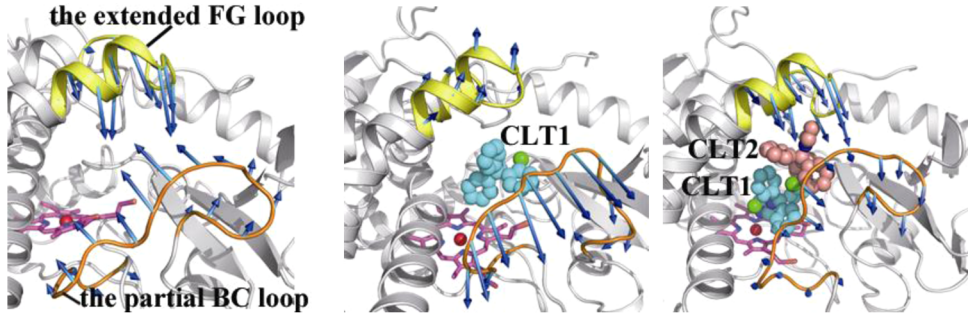

Figure 3. Collective motions corresponding to the PC1 for model I (A), model II (B), and model III (C). The arrow presents the motion direction, and the arrow length describes the motion magnitude.

3. RESULTS AND DISCUSSION

3.1. RMSD and RMSF Analyses. To observe conformation fluctuations of the whole system caused by the free dissociation of CLT, the root mean squared deviations (RMSD) of all Cα atoms and the root mean squared fluctuations (RMSF) of backbone atoms with respect to the initial structures were comparatively analyzed. As shown in Figure 2A, the Cα RMSD of model I quickly reaches equilibrium (~0.35 nm). The Cα RMSD of model II gradually increases to ~0.45 nm in the first 400 ns and then maintains at this plateau during the remainder of simulation time. The Cα RMSD of model III mainly stays at the first plateau (~0.35 nm) until 600 ns and then increases to the same plateau (~0.45 nm) as model II. These changes suggest that the dissociation of CLT would induce a great conformation change on the enzyme, and the presence of CLT2 slows the conformation change of enzyme caused by CLT1.

The RMSF as a function of residues is shown in Figure 2B. In model I, RMSF values of residues 73−88 (the partial BC loop) and residues 173−186 (the extended FG loop) reach to ~0.3 and ~0.4 nm, which are higher than other regions, showing that these regions are the most flexible. The partial BC loop of model II (RMSF 0.15−0.65 nm) is more flexible than that of model I (RMSF 0.10−0.34 nm). This is because the presence of CLT1 can hinder the formation of two hydrogen bonds between the S81 backbone NH and side chain OH and E184 carboxyl, which can form in model I (Figures S1 and S2, Supporting Information), enhancing the movement of the partial BC loop. The extended FG loop of model II (RMSF 0.10−0.27 nm) is more rigid than that of model I (RMSF 0.10−0.42 nm). One possible reason is that CLT1 can form a weak hydrogen bond with Q173 (Figure S2, Supporting Information), and this hydrogen bond would restrict the movement of the extended FG loop in model II. Compared to helix I of model I (Figure S1, Supporting Information), that of model II is observed to shift toward heme (Figure S2, Supporting Information), which is attributed to the hydrophobic interactions between the phenyl ring of CLT1 and L240, A241, and I244. The partial BC loop of model III (RMSF 0.10−0.24 nm) is more rigid than that of model II. This is because the addition of CLT2 pushes S81 to form a hydrogen bond with E78 (Figure S3A, Supporting Information), and this hydrogen bond promotes the structure change of residues 78−81 from a loose loop into a rigid helix. The extended FG loop of model III (RMSF 0.13−0.36 nm) is more flexible than that of model II. This is because the addition of CLT2 destroys the hydrogen bonds between D176 and T178, which can be found in model II (Figures S2 and S3A, Supporting Information), promoting the movement of the extended FG loop of model III. Clearly, the movements of the partial BC loop and the extended FG loop are influenced by the dissociation of CLT and may in turn affect the dissociation of CLT. The RMSF tendency from simulations is similar to that calculated from the B-factor values of crystal structure (Figure 2B), supporting that the molecule motions are well reproduced by our simulations.[35,36]

3.2. Collective Motions Revealed by PCA. To clarify the significant motions of enzymes induced by the dissociation of CLT, principal component analysis[37−39] (PCA) was performed on model I, model II, and model III. The first components (PC1), which represent the most significant motions of the models, account for ~43%, ~39%, and ~44% for model I, model II, and model III, respectively. Thus, the motions corresponding to PC1 should be emphasized.

As shown from the PC1 motion of model I (Figure 3A), the partial BC loop and the extended FG loop approach each other (closure of enzyme). This driving force may mainly originate from the hydrogen bond between S81 of the partial BC loop and E184 of the extended FG loop (Figure S1, Supporting Information). The minimum distance between the partial BC loop and the extended FG loop in the final equilibrated structure of model I is 0.19 nm, which is smaller than that in the ligand-free closed crystal structure (PDB code 2JJN,[18] 0.38 nm) and that in the ketoconazole-bound closed crystal structure (PDB code 2JJP,[18] 0.56 nm), demonstrating that the simulation of model I sampled the closed conformation.

For the PC1 motion of model II (Figure 3B), the partial BC loop and extended FG loop move away from each other (opening of enzyme), which is opposite to the closed motion of model I. This is because the addition of CLT1 hampers the formation of hydrogen bonds between S81 and E184 (Figure S2, Supporting Information), hindering the approach of the partial BC loop and the extended FG loop. Also, the addition of CLT1 would promote the separation of the partial BC loop and the extended FG loop through spatial repulsion. The above two aspects commonly drive the pocket formed by the partial BC loop and the extended FG loop adopts an opening motion. The minimum distance between the partial BC loop and the extended FG loop in the final equilibrated structure of model II is 0.35 nm, which is larger than that in the final equilibrated structure of model I, indicating that the simulation model II sampled the open conformation when compared to model I.

dx.doi.org/10.1021/ci400660e | J. Chem. Inf. Model. 2014, 54, 1218−1225

For the PC1 motion of model III (Figure 3C), the partial BC loop moves away from CLT molecules, while the extended FG loop approaches CLT molecules. Furthermore, the motional magnitude of the extended FG loop is larger than that of the partial BC loop in model III, causing the closure of enzyme. Actually, the motion direction of the partial BC loop in model III is similar to that in model II, while the motion direction of the extended FG loop in model III is opposite to that in model II. The possible reasons are that the addition of CLT2 pushes away the partial BC loop through spatial repulsion, and Q173, T178, and D179 of the extended FG loop can form hydrogen bonds with CLT2 from time to time, which drives the extended FG loop bend to CLT2 (Figure S3B–D, Supporting Information). This closing motion of model III would restrict the dissociation of CLT1, prolonging the residence time of CLT1 and promoting the inhibition efficiency.

3.3. Dissociation Landscape of Active Clotrimazole from Enzyme. *3.3.1. Without CLT2 (Model II).* To better understand the dissociation landscape of CLT1 without CLT2, which may be related to the inhibition efficiency of CLT1 against the enzyme, a set of configurations from the simulations are projected onto two coordinates to generate two-dimensional (2D) distribution landscapes, given in Figure 4A.

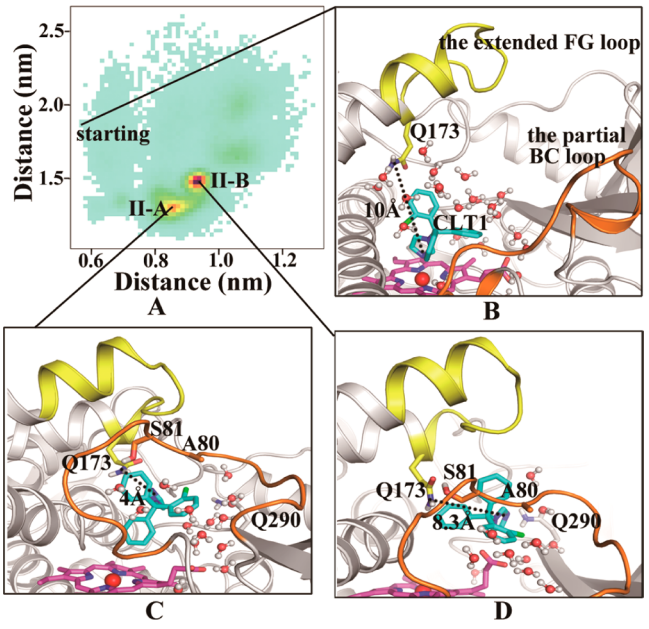

Figure 4. 2D Distribution landscape of CLT1 without CLT2 (Horizontal coordinate: center-of-mass distance between CLT1 and heme. Longitudinal coordinate: center-of-mass distance between the partial BC loop and the extended FG loop). As CLT1 quickly diffuses away from heme in model II, several extra short molecular dynamics (a total of ~70 ns) are carried out to better sample this landscape. (A). Darker color indicates higher population. Representative structures for the starting point (B), state II-A (C), and state II–B (D).

From the starting point to the state with the second maximum population (state II-A), the center-of-mass distance between CLT1 and heme increases from 0.58 to ~0.85 nm, the distance between heme iron and the CLT1 N3 atom (Fe–N3) increases from 0.23 to 1.03 nm, and the center-of-mass distance between the partial BC loop and the extended FG loop decreases from 1.90 to ~1.30 nm (Figure 4A), showing that CLT1 dissociates from heme, and the partial BC loop and the extended FG loop become close to each other. On one hand, in the starting point, the whole binding pocket adopts an open conformation that favors the dissociation of CLT1. On the other hand, the distance between the Q173 NE2 atom and the CLT1 N3 atom changes from 10 to 4 Å to generate a weak hydrogen bond (Figure 4B and C), thus the extended FG loop moves close to CLT1, indirectly leading to the closure of the extended FG loop and the partial BC loop. During this process (starting point→state II-A), water molecules penetrate from the entrance to the inside of the substrate binding site (Figure 4B and C), which may partially contribute to the dissociation of CLT1.

From state II-A to the state with the maximum population (state II–B), the center-of-mass distance between CLT1 and heme increases from ~0.85 to ~0.95 nm (Fe–N3 distance from 1.03 to 1.06 nm) and that between the partial BC loop and the extended FG loop increases from ~1.30 to ~1.50 nm (Figure 4A), showing that CLT1 continually dissociates from heme, and the partial BC loop and the extended FG loop move away from each other. Obviously, the motion of the partial BC loop and the extended FG loop during this step is in accordance with the motion corresponding to PC1. This is because the weak hydrogen bond between the Q173 NE2 atom and the CLT1 N3 atom was broken with their distance changing from 4 to 8.3 Å (Figure 4C and D), causing the extended FG loop to detach from CLT1, indirectly resulting in the opening of the partial BC loop and the extended FG loop. This opening motion may facilitate the continuous dissociation of CLT1. From state II-A to state II–B, the number of water molecules in the substrate binding site decreases from 13 to 11 (Figure 4C and D), which may be due to the opening of the partial BC loop and the extended FG loop. Shown in Table 1, the relative binding free energy ΔG_{bind} of CLT1 is calculated to be exothermic by 23.9 kcal/mol during this process. The electrostatic term (ΔE_{ele}) decreases by 39.4 kcal/mol, which is mainly because the CLT1 N3 atom is hydrogen-bonded to the Q290 NE2 atom with their distance decreasing from 7.8 to 3.1 Å. The noncovalent van der Waals term (ΔE_{vdw}) drops by 0.3 kcal/mol. One possible reason is that the center-of-mass distance between CLT1 and A80 decreases from 7.8 to 5.9 Å and that between CLT1 and S81 declines from 8.0 to 5.8 Å, suggesting that the interaction between CLT1 and the partial BC loop is strengthened.

To sum up, the starting point→state II-A→state II–B process describes the dissociation pathway of CLT1 in model II. CLT1 continually diffuses away from heme, and the partial BC loop and the extended FG loop first close and then open. This behavior can also be observed from time evolutions of the two coordinates of the 2D distribution landscape (Figures S4 and S5, Supporting Information).

3.3.2. With CLT2 Present (Model III). The dissociation landscape of CLT1 with CLT2 present is given in Figure 5A. From the starting point to the state with the second maximum population (state III-A), the center-of-mass distance between CLT1 and heme basically maintains at ~0.58 nm (Fe–N3 distance slightly increases from 0.23 to 0.27 nm) and that between the partial BC loop and the extended FG loop decreases from ~1.90 to ~1.57 nm, showing that CLT1 keeps close to heme, and the partial BC loop and the extended FG loop move close to each other. For one thing, in the starting point, the center-of-mass distance between the CLT2 Ring B and the CLT1 Ring A is 5.3 Å and that between the CLT2 Ring C and the CLT1 Ring C is 4.3 Å. In state III-A, the center-of-

dx.doi.org/10.1021/ci400660e | J. Chem. Inf. Model. 2014, 54, 1218–1225

Table 1. Relative Binding Free Energy Calculated by the MM-PBSA Method for CLT1 in Model II and Model III[a,b]

	model II		model III	
energy items (kcal/mol)	state II-A	state II-B	state III-A	state III-B
ΔE_{ele}	−23.3 ± 4.5	−62.6 ± 7.7	−25.8 ± 5.1	−33.1 ± 8.8
ΔE_{vdw}	−47.8 ± 2.4	−48.0 ± 4.1	−49.6 ± 2.5	−48.1 ± 3.0
ΔE_{gas}	−71.0 ± 4.3	−110.7 ± 6.4	−75.4 ± 4.8	−81.2 ± 8.5
$\Delta G_{nonpolar/PB}$	−4.0 ± 0.1	−4.0 ± 0.1	−4.0 ± 0.1	−4.0 ± 0.1
$\Delta G_{polar/PB}$	4.1 ± 2.7	19.9 ± 2.9	35.6 ± 2.7	25.6 ± 3.8
$\Delta G_{sol/PB}$	0.2 ± 2.7	15.9 ± 2.9	31.6 ± 2.7	21.6 ± 3.8
ΔG_{bind}	−70.9 ± 4.1	−94.8 ± 6.0	−43.7 ± 5.2	−59.6 ± 8.1

[a] $\Delta E_{gas} = \Delta E_{ele} + \Delta E_{vdw}$, $\Delta G_{sol/PB} = \Delta G_{nonpolar/PB} + \Delta G_{polar/PB}$, $\Delta G_{bind} = \Delta E_{gas} + \Delta G_{sol/PB}$ [b] In model III, the complex of enzyme and CLT2 is considered as receptor

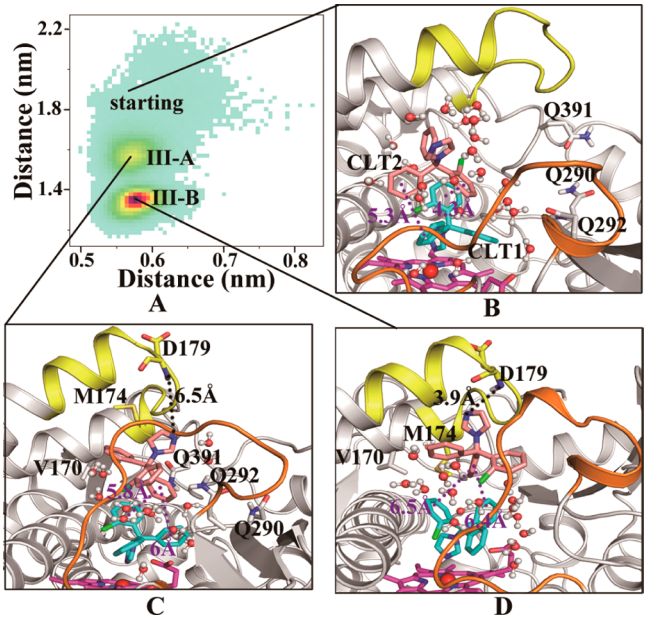

Figure 5. 2D Distribution landscape of CLT1 with CLT2 present (A). Representative structures for the starting point (B), state III-A (C), and state III−B (D).

mass distance between the CLT2 Ring A and the CLT1 Ring B is 6 Å and that between the CLT2 Ring A and the CLT1 Ring C is 5.8 Å. These suggest that CLT2 can directly stabilize CLT1 through $\pi-\pi$ stacking interactions.[35,36] For another, CLT2 induces the approach of Q290 and Q292 of β4 and Q391 of the C terminal, and these residues help to stabilize the phenyl ring of CLT1. Together, the above two factors are responsible for the positional and orientational stabilization of CLT1. The approach of the partial BC loop and the extended FG loop may be driven by the simultaneous interactions of CLT2 with the partial BC loop (e.g., P73, T74, G79, A80, S81, and T83) and the extended FG loop (e.g., Q173, P177, T178, and I186). From the starting point to state III-A, water molecules penetrate from the entrance into the inside of the substrate binding site (Figure 5B and C), and this may be slightly favorable for the dissociation of CLT.

From state III-A to the state with the maximum population (state III−B), the center-of-mass distance between CLT1 and heme basically stays at ∼0.58 nm (Fe−N3 distance slightly decreases from 0.27 to 0.25 nm) and that between the partial BC loop and the extended FG loop decreases from ∼1.57 to ∼1.37 nm (Figure 5A), showing that CLT1 still keeps close to heme, and the partial BC loop and the extended FG loop continually move close to each other to produce a closed conformation. Apparently, the motion of the partial BC loop and the extended FG loop during this process agrees well with the motion direction along PC1. This closed structure may extend the residence time of CLT molecules and thus improve the inhibition efficiency. The possible reason responsible for the continuous approach of the partial BC loop and the extended FG loop is that the distance between the D179 N atom and the CLT2 N3 atom changes from 6.5 to 3.9 Å to produce a weak hydrogen bond (Figure 5C and D). This hydrogen bond promotes the extended FG loop bend toward CLT2, indirectly causing the closure of the extended FG loop and the partial BC loop. The center-of-mass distances between the CLT2 Ring A and the CLT1 Ring B slightly increases from 6 to 6.4 Å and that between the CLT2 Ring A and the CLT1 Ring C slightly rises from 5.8 to 6.5 Å (Figure 5C and D), suggesting that there are still $\pi-\pi$ stacking interactions between CLT1 and CLT2. Besides, the bending of the extended FG loop induced by CLT2 promotes V170 and M174 to interact with the chlorophenyl ring of CLT1. These two aspects help to stabilize the position of CLT1. From state III-A to state III−B, the number of water molecules in the cavity between CLT1 and CLT2 increases from 9 to 12 (Figure 5C and D), which may promote the dissociation of CLT2 and impede the diffusion of CLT1 from the active site. Shown in Table 1, ΔG_{bind} of CLT1 is exothermic by 15.9 kcal/mol in this process. Particularly, the electrostatic term (ΔE_{ele}) decreases by 7.3 kcal/mol. This is because the distance between the CLT1 N3 atom and heme iron atom slightly decreases from 2.7 to 2.5 Å, enhancing the interaction between CLT1 and heme iron. The noncovalent van der Waals term (ΔE_{vdw}) slightly rises by 1.5 kcal/mol. The possible reason is that during this process the center-of-mass distance between the CLT2 Ring A and the CLT1 Ring B increases by 0.4 Å and that between the CLT2 Ring A and the CLT1 Ring C rises by 0.7 Å, slightly weakening the interaction between CLT1 and CLT2.

Collectively, the starting point→state III-A→state III−B process describes the dissociation pathway of CLT1 in model III. CLT1 basically keeps close to heme, and the partial BC loop and the extended FG loop move close to each other. This phenomenon can also be observed from the time evolutions of the two coordinates of the 2D distribution landscape (Figures S4 and S5, Supporting Information).

A comparison between model II and model III indicates that the presence of CLT2 would constrain the dissociation of CLT1 through the $\pi-\pi$ stacking interactions between them.

3.3.3. Model III-Post. From the analyses of model III, we have known that the dissociation of CLT1 can be restricted through the direct $\pi-\pi$ stacking interactions exerted by CLT2

and the rearranged binding site induced by CLT2. To further clarify the influence of these two factors on the dissociation of CLT1, model III-post-1, which starts from the end of the 1 μs simulation of model III and deletes CLT2, was employed a 100 ns simulation. The corresponding 2D distribution landscape is presented in Figure 6. From the starting point to the state with

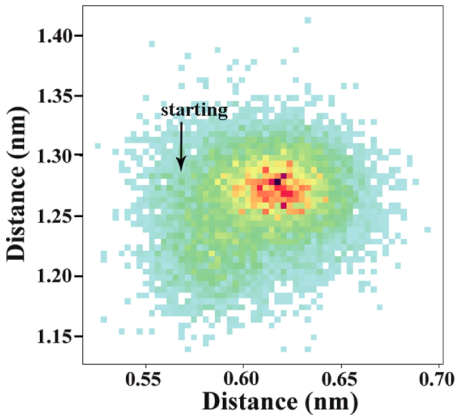

Figure 6. 2D Distribution landscape of model III-post-1.

maximum population, the center-of-mass distance between CLT1 and heme slightly increases from 0.58 to ~0.62 nm, and that between the partial BC loop and the extended FG loop negligibly decreases from ~1.29 to ~1.28 nm, showing that even without CLT2, CLT1 can still keep close to heme, and the distance between the partial BC loop and the extended FG loop is relatively steady. However, in model II, the center-of-mass distance between CLT1 and heme quickly rises from 0.58 to ~1.10 nm in the first 10 ns, showing that CLT1 quickly and significantly dissociates from heme. These different dissociation behaviors of CLT1 between model III-post-1 and model II can be attributed to their different starting structures. Compared to the starting structure of model II, V170 and M174 of the extended FG loop in model III-post-1 interact more with the chlorophenyl ring of CLT1 (Figure 7), which can be attributed

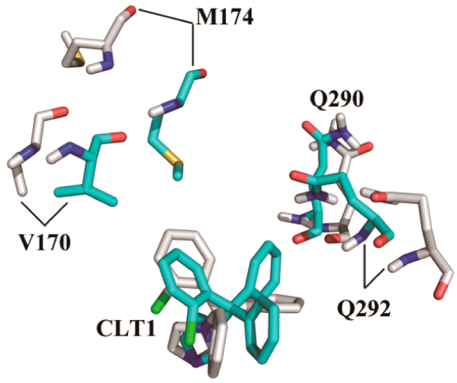

Figure 7. Interactions between CLT1 and some key residues in the starting structures of model III-post-1 (cyan) and model II (white).

to the bending of the extended FG loop induced by the hydrogen bond between CLT2 and D179 during the simulation of model III. Additionally, Q290 and Q292 of model III-post-1 interact more with the phenyl ring of CLT1 (Figure 7) because CLT2 induces Q290 and Q292 to approach CLT1 during the simulation of model III.

A comparison of model II and model III-post-1 shows that even without the $\pi-\pi$ stacking interactions exerted by CLT2 on CLT1 the rearranged binding site previously induced by CLT2 impedes the dissociation of CLT1, indicating that the rearranged binding site becomes the main factor to restrict the dissociation of CLT1 in the later stage.

To observe how the presence of CLT1 arranges the protein structure around CLT2, model III-post-2 (starting from the end of the 1 μs simulation of model III and deleting CLT1) and model III-continue (starting from the end of the 1 μs simulation of model III) were separately employed 100 ns simulations. As shown in Figure S6 of the Supporting Information, the RMSD value of the partial BC loop and the extended FG loop in model III-post-2 fluctuates around 0.20 nm, while that of model III-continue remains around 0.17 nm, indicating that the presence of CLT1 can help to stabilize the protein structure around CLT2. The superposition of the initial and the final snapshots reveals that in model-III-continue CLT1 interacts with M86 of the partial BC loop and Q173 and M174 of the extended FG loop, restricting the movements of these residues (Figure S7A, Supporting Information), while in model-III-post-2, the movements of these residues are enhanced, owing to the lack of the interaction with CLT1 (Figure S7B, Supporting Information).

CONCLUSIONS

In this work, the free dissociation processes of clotrimazole from P450 in several models have been comparatively investigated by MD simulations. Several conclusions were drawn.

The RMSF analyses suggest that the active clotrimazole (CLT1) can enhance the flexibility of the partial BC loop and rigidify the extended FG loop, whereas the effector clotrimazole (CLT2) can rigidify the partial BC loop and promote the movement of the extended FG loop. The PCA analyses reveal that CLT1 can facilitate the opening motion of the partial BC loop and the extended FG loop of model II due to the breaking of the hydrogen bond between S81 and E184 and the spatial repulsion, while CLT2 can promote model III to adopt the closing motion owing to the formation of the transient hydrogen bonds between CLT2 and the extended FG loop (Q173, T178 and D179). This closing motion may in turn restrict the dissociation of CLT1.

The dissociation landscapes of CLT1 show that when P450 only binds to CLT1 (model II), CLT1 continually diffuses away from heme, and the partial BC loop and the extended FG loop first close and then open. When P450 binds to two CLT molecules (model III), CLT1 basically keeps close to heme, and the partial BC loop and the extended FG loop move close to each other. In the dissociation process of CLT1, CLT2 plays a cooperative-action role. CLT2 blocks CLT1 first through $\pi-\pi$ stacking interaction and then through inducing Q290 and Q292 to approach the phenyl ring of CLT1 and promoting V170 and M174 to interact with the chlorophenyl ring of CLT1 by a weak hydrogen bond between CLT2 and D179 (the rearranged binding site). The presence of CLT1 can help to stabilize the protein structure around CLT2 by interacting with M86, Q173, and M174.

ASSOCIATED CONTENT

Supporting Information

Typical snapshots, time evolutions of the center-of-mass distances between CLT1 and heme and between the partial

dx.doi.org/10.1021/ci400660e | J. Chem. Inf. Model. 2014, 54, 1218−1225

BC loop and extended FG loop, all-atom RMSD of the partial BC loop and extended FG loop for Model III-post-2 and Model III-continue, and superposition of the starting snapshot and end snapshot for model-III-continue and model-III-post-2. This material is available free of charge via the Internet at http://pubs.acs.org.

AUTHOR INFORMATION

Corresponding Authors

*Tel./Fax: +86-771-3233718. E-mail: jianyiwang@gxu.edu.cn (J.W.)

*Tel./Fax: +86-771-3233718. E-mail: zqliang@gxu.edu.cn (Z.L.).

Author Contributions

‖These two authors (M. Wang and M. Baaden) contributed equally to this work.

Notes

The authors declare no competing financial interest.

ACKNOWLEDGMENTS

This work is supported by the Project of Guangxi Natural Science Foundation (2013GXNSFBA019152), National Natural Science Foundation of China (21262004), Key Scientific Research Project of Guangxi Natural Science Foundation (2012GXNSFDA053002), and "Initiative d'Excellence" program from the French State (Grant "DYNAMO", ANR-11-LABX-0011). The computational resources are partly provided by Multifunction Computer Center of Guangxi University.

REFERENCES

(1) Denisov, I. G.; Makris, T. M.; Sligar, S. G.; Schlichting, I. Structure and chemistry of cytochrome P450. *Chem. Rev.* **2005**, *105*, 2253−2277.

(2) Schuster, I.; Bernhardt, R. Inhibition of cytochromes p450: Existing and new promising therapeutic targets. *Drug Metab. Rev.* **2007**, *39*, 481−499.

(3) Wienkers, L. C.; Heath, T. G. Predicting in vivo drug interactions from in vitro drug discovery data. *Nat. Rev. Drug Discovery* **2005**, *4*, 825−833.

(4) Lamb, D. C.; Waterman, M. R.; Kelly, S. L.; Guengerich, F. P. Cytochromes P450 and drug discovery. *Curr. Opin. Biotechnol.* **2007**, *18*, 504−512.

(5) Piscitelli, S. C.; Flexner, C.; Minor, J. R.; Polis, M. A.; Masur, H. Drug interactions in patients infected with human immunodeficiency virus. *Clin. Infect. Dis.* **1996**, *23*, 685−693.

(6) Danton, A. C.; Montastruc, F.; Sommet, A.; Durrieu, G.; Bagheri, H.; Bondon-Guitton, E.; Lapeyre-Mestre, M.; Montastruc, J. L. Importance of cytochrome P450 (CYP450) in adverse drug reactions due to drug-drug interactions: a PharmacoVigilance study in France. *Eur. J. Clin. Pharmacol.* **2013**, *69*, 885−888.

(7) Cameron, M. D.; Wen, B.; Roberts, A. G.; Atkins, W. M.; Campbell, A. P.; Nelson, S. D. Cooperative binding of acetaminophen and caffeine within the P450 3A4 active site. *Chem. Res. Toxicol.* **2007**, *20*, 1434−1441.

(8) Isin, E. M.; Guengerich, F. P. Kinetics and thermodynamics of ligand binding by cytochrome P450 3A4. *J. Biol. Chem.* **2006**, *281*, 9127−9136.

(9) Denisov, I. G.; Frank, D. J.; Sligar, S. G. Cooperative properties of cytochromes P450. *Pharmacol. Ther.* **2009**, *124*, 151−167.

(10) Harrelson, J. P.; Atkins, W. M.; Nelson, S. D. Multiple-ligand binding in CYP2A6: probing mechanisms of cytochrome P450 cooperativity by assessing substrate dynamics. *Biochemistry* **2008**, *47*, 2978−2988.

(11) Hartman, J. H.; Bradley, A. M.; Laddusaw, R. M.; Perry, M. D., Jr.; Miller, G. P. Structure of pyrazole derivatives impact their affinity, stoichiometry, and cooperative interactions for CYP2E1 complexes. *Arch. Biochem. Biophys.* **2013**, *537*, 12−20.

(12) Sohl, C. D.; Isin, E. M.; Eoff, R. L.; Marsch, G. A.; Stec, D. F.; Guengerich, F. P. Cooperativity in oxidation reactions catalyzed by cytochrome P450 1A2: Highly cooperative pyrene hydroxylation and multiphasic kinetics of ligand binding. *J. Biol. Chem.* **2008**, *283*, 7293−7308.

(13) Sadeghi, S. J.; Ferrero, S.; Di Nardo, G.; Gilardi, G. Drug-drug interactions and cooperative effects detected in electrochemically driven human cytochrome P450 3A4. *Bioelectrochemistry* **2012**, *86*, 87−91.

(14) Isin, E. M.; Sohl, C. D.; Eoff, R. L.; Guengerich, F. P. Cooperativity of cytochrome P450 1A2: Interactions of 1,4-phenylene diisocyanide and 1-isopropoxy-4-nitrobenzene. *Arch. Biochem. Biophys.* **2008**, *473*, 69−75.

(15) Collom, S. L.; Laddusaw, R. M.; Burch, A. M.; Kuzmic, P.; Perry, M. D., Jr.; Miller, G. P. CYP2E1 substrate inhibition. Mechanistic interpretation through an effector site for monocyclic compounds. *J. Biol. Chem.* **2008**, *283*, 3487−3496.

(16) Ekroos, M.; Sjogren, T. Structural basis for ligand promiscuity in cytochrome P450 3A4. *Proc. Natl. Acad. Sci. U.S.A.* **2006**, *103*, 13682−13687.

(17) Zhao, Y.; White, M. A.; Muralidhara, B. K.; Sun, L.; Halpert, J. R.; Stout, C. D. Structure of microsomal cytochrome P450 2B4 complexed with the antifungal drug bifonazole: Insight into P450 conformational plasticity and membrane interaction. *J. Biol. Chem.* **2006**, *281*, 5973−5981.

(18) Montemiglio, L. C.; Gianni, S.; Vallone, B.; Savino, C. Azole drugs trap cytochrome P450 EryK in alternative conformational states. *Biochemistry* **2010**, *49*, 9199−9206.

(19) Savino, C.; Montemiglio, L. C.; Sciara, G.; Miele, A. E.; Kendrew, S. G.; Jemth, P.; Gianni, S.; Vallone, B. Investigating the structural plasticity of a cytochrome P450: Three-dimensional structures of P450 EryK and binding to its physiological substrate. *J. Biol. Chem.* **2009**, *284*, 29170−29179.

(20) Bren, U.; Oostenbrink, C. Cytochrome P450 3A4 inhibition by ketoconazole: Tackling the problem of ligand cooperativity using molecular dynamics simulations and free-energy calculations. *J. Chem. Inf. Model.* **2012**, *52*, 1573−1582.

(21) Fishelovitch, D.; Hazan, C.; Shaik, S.; Wolfson, H. J.; Nussinov, R. Structural dynamics of the cooperative binding of organic molecules in the human cytochrome P450 3A4. *J. Am. Chem. Soc.* **2007**, *129*, 1602−1611.

(22) Fishelovitch, D.; Hazan, C.; Hirao, H.; Wolfson, H. J.; Nussinov, R.; Shaik, S. QM/MM study of the active species of the human cytochrome P450 3A4, and the influence thereof of the multiple substrate binding. *J. Phys. Chem. B* **2007**, *111*, 13822−13832.

(23) Li, J.; Wei, D. Q.; Wang, J. F.; Li, Y. X. A negative cooperativity mechanism of human CYP2E1 inferred from molecular dynamics simulations and free energy calculations. *J. Chem. Inf. Model.* **2011**, *51*, 3217−3225.

(24) Van Der Spoel, D.; Lindahl, E.; Hess, B.; Groenhof, G.; Mark, A. E.; Berendsen, H. J. GROMACS: Fast, flexible, and free. *J. Comput. Chem.* **2005**, *26*, 1701−1718.

(25) Pronk, S.; Pall, S.; Schulz, R.; Larsson, P.; Bjelkmar, P.; Apostolov, R.; Shirts, M. R.; Smith, J. C.; Kasson, P. M.; van der Spoel, D.; Hess, B.; Lindahl, E. GROMACS 4.5: A high-throughput and highly parallel open source molecular simulation toolkit. *Bioinformatics* **2013**, *29*, 845−854.

(26) van Gunsteren, W. F.; Billeter, S.; Eising, A.; Hünenberger, P.; Krüger, P.; Mark, A.; Scott, W.; Tironi, I. *Biomolecular Simulation: The GROMOS96 Manual and User Guide*; Vdf Hochschul-verlag AG an der ETH Zürich: Zürich, Switzerland, 1996.

(27) Malde, A. K.; Zuo, L.; Breeze, M.; Stroet, M.; Poger, D.; Nair, P. C.; Oostenbrink, C.; Mark, A. E. An automated force field topology builder (ATB) and repository, version 1.0. *J. Chem. Theory Comput.* **2011**, *7*, 4026−4037.

(28) Berendsen, H. J. C.; Postma, J. P. M.; van Gunsteren, E. F.; Hermans, J. *Intermolecular Forces*; Pullman, B., Ed.; Reidel: Dordrecht, The Netherlands, 1981.
(29) Bussi, G.; Donadio, D.; Parrinello, M. Canonical sampling through velocity rescaling. *J. Chem. Phys.* **2007**, *126*, 014101.
(30) Parrinello, M.; Rahman, A. Polymorphic transitions in single crystals: A new molecular dynamics method. *J. Appl. Phys.* **1981**, *52*, 7182−7190.
(31) Hess, B.; Bekker, H.; Berendsen, H. J. C.; Fraaije, J. G. E. M. LINCS: A linear constraint solver for molecular simulations. *J. Comput. Chem.* **1997**, *18*, 1463−1472.
(32) Essmann, U.; Perera, L.; Berkowitz, M. L.; Darden, T.; Lee, H.; Pedersen, L. G. A smooth particle mesh Ewald method. *J. Chem. Phys.* **1995**, *103*, 8577.
(33) Kollman, P. A.; Massova, I.; Reyes, C.; Kuhn, B.; Huo, S.; Chong, L.; Lee, M.; Lee, T.; Duan, Y.; Wang, W.; Donini, O.; Cieplak, P.; Srinivasan, J.; Case, D. A.; Cheatham, T. E. Calculating structures and free energies of complex molecules: Combining molecular mechanics and continuum models. *Acc. Chem. Res.* **2000**, *33*, 889−897.
(34) Brandsdal, B. O.; Osterberg, F.; Almlof, M.; Feierberg, I.; Luzhkov, V. B.; Aqvist, J. Free energy calculations and ligand binding. *Adv. Protein Chem.* **2003**, *66*, 123−158.
(35) Graf, M. M.; Bren, U.; Haltrich, D.; Oostenbrink, C. Molecular dynamics simulations give insight into D-glucose dioxidation at C2 and C3 by *Agaricus meleagris* pyranose dehydrogenase. *J. Comput.-Aided Mol. Des.* **2013**, *27*, 295−304.
(36) Ohmura, T.; Ueda, T.; Ootsuka, K.; Saito, M.; Imoto, T. Stabilization of hen egg white lysozyme by a cavity-filling mutation. *Protein Sci.* **2001**, *10*, 313−320.
(37) Amadei, A.; Linssen, A. B. M.; Berendsen, H. J. C. Essential dynamics of proteins. *Proteins: Struct., Funct., Bioinf.* **1993**, *17*, 412−425.
(38) Mu, Y.; Nguyen, P. H.; Stock, G. Energy landscape of a small peptide revealed by dihedral angle principal component analysis. *Proteins: Struct., Funct., Bioinf.* **2005**, *58*, 45−52.
(39) Friedman, A. J.; Durrant, J. D.; Pierce, L. C.; McCorvie, T. J.; Timson, D. J.; McCammon, J. A. The molecular dynamics of *Trypanosoma brucei* UDP-galactose 4′-epimerase: A drug target for African sleeping sickness. *Chem. Biol. Drug Des.* **2012**, *80*, 173−181.